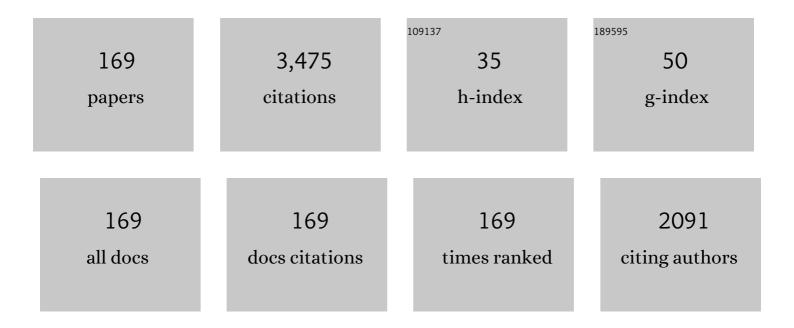
List of Publications by Year in descending order

Source: https://exaly.com/author-pdf/3878317/publications.pdf Version: 2024-02-01



DEBAIVOTI DAS

#	Article	IF	CITATIONS
1	Photoluminescence phenomena prevailing in c-axis oriented intrinsic ZnO thin films prepared by RF magnetron sputtering. RSC Advances, 2014, 4, 35735-35743.	1.7	176
2	Generally Applicable Self-Masked Dry Etching Technique for Nanotip Array Fabrication. Nano Letters, 2004, 4, 471-475.	4.5	147
3	Photocatalytic degradation of Rhodamine-B dye by stable ZnO nanostructures with different calcination temperature induced defects. Applied Surface Science, 2019, 465, 546-556.	3.1	127
4	A novel preparation technique for preparing hydrogenated amorphous silicon with a more rigid and stable Si network. Applied Physics Letters, 1991, 59, 1096-1098.	1.5	108
5	Properties of electron-beam-evaporated tin oxide films. Thin Solid Films, 1987, 147, 321-331.	0.8	96
6	Self-doped TiO2 nanowires in TiO2-B single phase, TiO2-B/anatase and TiO2-anatase/rutile heterojunctions demonstrating individual superiority in photocatalytic activity under visible and UV light. Applied Surface Science, 2018, 455, 1106-1115.	3.1	67
7	Properties of tin oxide films prepared by reactive electron beam evaporation. Thin Solid Films, 1987, 149, 291-301.	0.8	65
8	Nanocrystalline silicon films prepared from silane plasma in RF-PECVD, using helium dilution without hydrogen: structural and optical characterization. Nanotechnology, 2007, 18, 415704.	1.3	65
9	Narrow Band-Gap a-Si:H with Improved Minority Carrier-Transport Prepared by Chemical Annealing. Japanese Journal of Applied Physics, 1991, 30, L239-L242.	0.8	64
10	Characterization of the Si:H network during transformation from amorphous to micro- and nanocrystalline structures. Journal of Applied Physics, 2006, 100, 103701.	1.1	54
11	Low temperature grown ZnO:Ga films with predominant c-axis orientation in wurtzite structure demonstrating high conductance, transmittance and photoluminescence. RSC Advances, 2016, 6, 6144-6153.	1.7	53
12	Characterization of tin doped indium oxide films prepared by electron beam evaporation. Solar Energy Materials and Solar Cells, 1986, 13, 11-23.	0.4	51
13	Conducting wide band gap nc-Si/a-SiC:H films for window layers in nc-Si solar cells. Journal of Materials Chemistry A, 2013, 1, 14744.	5.2	50
14	Electrical transport phenomena prevailing in undoped nc-Si/a-SiNx:H thin films prepared by inductively coupled plasma chemical vapor deposition. Journal of Applied Physics, 2013, 114, .	1.1	50
15	Control of hydrogenation and modulation of the structural network in Si:H by interrupted growth and H-plasma treatment. Physical Review B, 1995, 51, 10729-10736.	1.1	49
16	Wide optical-gap a-SiO:H films prepared by rf glow discharge. Journal of Non-Crystalline Solids, 1997, 210, 148-154.	1.5	47
17	Transparent and conducting intrinsic ZnO thin films prepared at high growth-rate with c-axis orientation and pyramidal surface texture. Applied Surface Science, 2013, 286, 397-404.	3.1	46
18	ZnO-Cu O heterostructure photocatalyst for efficient dye degradation. Journal of Physics and Chemistry of Solids, 2020, 143, 109463.	1.9	46

#	Article	IF	CITATIONS
19	Infrared vibrational spectra of hydrogenated amorphous silicon carbide thin films prepared by glow discharge. Solar Energy Materials and Solar Cells, 1987, 15, 45-57.	0.4	45
20	Controlling the growth of nanocrystalline silicon by tuning negative substrate bias. Solar Energy Materials and Solar Cells, 2011, 95, 3181-3188.	3.0	45
21	Tunable photoluminescence from nc-Si/a-SiNx:H quantum dot thin films prepared by ICP-CVD. Physical Chemistry Chemical Physics, 2013, 15, 3881.	1.3	45
22	Optimization of Si doping in ZnO thin films and fabrication of n-ZnO:Si/p-Si heterojunction solar cells. Journal of Alloys and Compounds, 2020, 824, 153902.	2.8	45
23	Heterogeneity in microcrystalline-transition state: Origin of Si-nucleation and microcrystallization at higher rf power from Ar-diluted SiH4 plasma. Journal of Applied Physics, 2001, 89, 3041-3048.	1.1	44
24	Characterization of undoped μc-SiO:H films prepared from (SiH4+CO2+H2)-plasma in RF glow discharge. Solar Energy Materials and Solar Cells, 2000, 63, 285-297.	3.0	43
25	Studies on the structural properties of SiO:H films prepared from (SiH4+CO2+He) plasma in RF-PECVD. Solar Energy Materials and Solar Cells, 2009, 93, 588-596.	3.0	42
26	Nanocrystalline silicon thin films prepared by low pressure planar inductively coupled plasma. Applied Surface Science, 2013, 276, 249-257.	3.1	42
27	Role of hydrogen in controlling the growth of μc-Si:H films from argon diluted SiH4 plasma. Journal of Applied Physics, 2002, 91, 5442-5448.	1.1	41
28	Structural studies on Si:H network by Raman, micro-photoluminescence, electron microscopy and ultraviolet ellipsometry: effect of Ar dilution to the SiH4-plasma. Thin Solid Films, 2005, 476, 237-245.	0.8	41
29	ZnO/CdS/CuS heterostructure: A suitable candidate for applications in visible-light photocatalysis. Journal of Physics and Chemistry of Solids, 2022, 160, 110344.	1.9	41
30	Micro-Raman and ultraviolet ellipsometry studies on μc-Si:H films prepared by H2 dilution to the Ar-assisted SiH4 plasma in radio frequency glow discharge. Journal of Applied Physics, 2003, 93, 2528-2535.	1.1	39
31	A novel approach towards silicon nanotechnology. Journal Physics D: Applied Physics, 2003, 36, 2335-2346.	1.3	39
32	Quantum confinement effects in nano-silicon thin films. Solid State Communications, 1998, 108, 983-987.	0.9	38
33	Anti-reflection coatings for silicon solar cells from hydrogenated diamond like carbon. Applied Surface Science, 2015, 345, 204-215.	3.1	38
34	Superior photocatalytic dye degradation under visible light by reduced graphene oxide laminated TiO2-B nanowire composite. Journal of Environmental Chemical Engineering, 2019, 7, 103358.	3.3	37
35	Effect of deposition temperature on the growth of nanocrystalline silicon network from helium diluted silane plasma. Journal Physics D: Applied Physics, 2008, 41, 155420.	1.3	36
36	Correlation between the physical parameters of the i –nc-Si absorber layer grown by 27.12 MHz plasma with the nc-Si solar cell parameters. Applied Surface Science, 2017, 416, 980-987.	3.1	36

#	Article	IF	CITATIONS
37	Properties of a-SiO:H films prepared by RF glow discharge. Solar Energy Materials and Solar Cells, 2000, 60, 167-179.	3.0	35
38	Hydrogen induced promotion of nanocrystallization from He-diluted SiH <sub>4</sub> plasma. Journal Physics D: Applied Physics, 2008, 41, 085303.	1.3	35
39	Photoluminescent silicon quantum dots in core/shell configuration: synthesis by low temperature and spontaneous plasma processing. Nanotechnology, 2011, 22, 055601.	1.3	35
40	Further improvements in conducting and transparent properties of ZnO:Ga films with perpetual c -axis orientation: Materials optimization and application in silicon solar cells. Applied Surface Science, 2017, 411, 315-320.	3.1	35
41	Reduced Graphene Oxide-Laminated One-Dimensional TiO <sub>2</sub> –Bronze Nanowire Composite: An Efficient Photoanode Material for Dye-Sensitized Solar Cells. ACS Omega, 2021, 6, 4362-4373.	1.6	34
42	Enhancement of multiferroic properties and unusual magnetic phase transition in Eu doped bismuth ferrite nanoparticles. New Journal of Chemistry, 2017, 41, 10985-10991.	1.4	33
43	Synthesis of diameter controlled multiwall carbon nanotubes by microwave plasma-CVD on low-temperature and chemically processed Fe nanoparticle catalysts. Applied Surface Science, 2020, 515, 146043.	3.1	31
44	Narrow band gap reduced TiO2-B:Cu nanowire heterostructures for efficient visible light absorption, charge separation and photocatalytic degradation. Applied Surface Science, 2020, 506, 144880.	3.1	29
45	Development of nc-Si/ <i>a</i> -SiN <i><sub>x</sub></i> :H Thin Films for Photovoltaic and Light-Emitting Applications. Science of Advanced Materials, 2013, 5, 188-198.	0.1	28
46	Helium versus hydrogen dilution in the optimization of polymorphous silicon solar cells. Journal of Non-Crystalline Solids, 2004, 338-340, 668-672.	1.5	26
47	Realizing a variety of carbon nanostructures at low temperature using MW-PECVD of (CH4+H2) plasma. Applied Surface Science, 2013, 273, 806-815.	3.1	26
48	Nanocrystalline silicon thin films from SiH 4 plasma diluted by H 2 and He in RF-PECVD. Journal of Physics and Chemistry of Solids, 2017, 105, 90-98.	1.9	26
49	Control of Crystallization at Low Thickness in µc-Si:H Films Using Layer-by-Layer Growth Scheme. Japanese Journal of Applied Physics, 1999, 38, L1087-L1090.	0.8	24
50	Ternary ZnCdSO composite photocatalyst for efficient dye degradation under visible light retaining Z-scheme of migration pathways for the photogenerated charge carriers. Solar Energy Materials and Solar Cells, 2020, 217, 110674.	3.0	24
51	Effect of hydrogen in controlling the structural orientation of ZnO:Ga:H as transparent conducting oxide films suitable for applications in stacked layer devices. Physical Chemistry Chemical Physics, 2016, 18, 20450-20458.	1.3	22
52	Promotion of microcrystallization by argon in moderately hydrogen diluted silane plasma. Solar Energy Materials and Solar Cells, 2002, 74, 407-413.	3.0	21
53	Further improvements of nano-diamond structures on unheated substrates by optimization of parameters with secondary plasma in MW-PECVD. Surface and Coatings Technology, 2015, 272, 357-365.	2.2	21
54	SiOx nanowires with intrinsic nC-Si quantum dots: the enhancement of the optical absorption and photoluminescence. Journal of Materials Chemistry C, 2013, 1, 6623.	2.7	20

#	Article	IF	CITATIONS
55	Low temperature growth of carbon nanotubes by microwave plasma stimulated by CO2 as weak oxidant and guided by shadow masking. Diamond and Related Materials, 2018, 88, 204-214.	1.8	20
56	Further optimization of ITO films at the melting point of Sn and configuration of Ohmic contact at the c-Si/ITO interface. Applied Surface Science, 2019, 481, 16-24.	3.1	20
57	Improved TCO characteristics of ZnO:Si films via utilization of Si4+ ionized donor states and its application in n-SZO/p-Si heterojunction solar cells. Solar Energy Materials and Solar Cells, 2020, 206, 110278.	3.0	20
58	Autogenic single p/n-junction solar cells from black-Si nano-grass structures of p-to-n type self-converted electronic configuration. Nanoscale, 2020, 12, 15371-15382.	2.8	20
59	Graphitic carbon nitride (g-C3N4) incorporated TiO2–B nanowires as efficient photoanode material in dye sensitized solar cells. Materials Chemistry and Physics, 2021, 266, 124520.	2.0	19
60	Morphological variations of ZnO nanostructures and its influence on the photovoltaic performance when used as photoanodes in dye sensitized solar cells. Solar Energy Materials and Solar Cells, 2022, 243, 111811.	3.0	19
61	Quantum size effects on the optical properties of nc-Si QDs embedded in an a-SiO <sub>x</sub> matrix synthesized by spontaneous plasma processing. Physical Chemistry Chemical Physics, 2015, 17, 5063-5071.	1.3	18
62	Synthesis of CdS/GO modified ZnO heterostructure for visible light dye degradation applications. Applied Surface Science, 2021, 570, 151260.	3.1	18
63	Correlation of Electrical, Thermal and Structural Properties of Microcrystalline Silicon Thin Films. Japanese Journal of Applied Physics, 2002, 41, L229-L232.	0.8	17
64	Size effect on electronic transport in nC–Si/SiO core/shell quantum dots. Materials Research Bulletin, 2012, 47, 3625-3629.	2.7	17
65	Melting point of Sn as the optimal growth temperature in realizing the favored transparent conducting properties of In2O3:Sn films. Journal of Alloys and Compounds, 2018, 767, 642-650.	2.8	17
66	CdS Q-Dot-Impregnated TiO <sub>2</sub> -B Nanowire-Based Photoanodes for Efficient Photovoltaic Conversion in †Q-Dot Co-sensitized DSSC'. Energy & Fuels, 2021, 35, 8246-8262.	2.5	17
67	Synthesis of nanocrystalline diamond embedded diamond-like carbon films on untreated glass substrates at low temperature using (C2H2Â+ÂH2) gas composition in microwave plasma CVD. Applied Surface Science, 2022, 579, 152132.	3.1	17
68	Two-Step Visible Light Photocatalytic Dye Degradation Phenomena in Ag <sub>2</sub> O-Impregnated ZnO Nanorods via Growth of Metallic Ag and Formation of ZnO/Ag <sup>0</sup> /Ag <sub>2</sub> O Heterojunction Structures. Langmuir, 2022, 38, 4503-4520.	1.6	17
69	Microstructural association of diverse chemical constituents in nc-SiOx:H network synthesized by spontaneous low temperature plasma processing. Physica E: Low-Dimensional Systems and Nanostructures, 2018, 103, 99-109.	1.3	16
70	Wide optical gap B-doped nc-Si thin films with advanced crystallinity and conductivity on transparent flexible substrates for potential low-cost flexible electronics including nc-Si superstrate p–i–n solar cells. Materials Advances, 2021, 2, 2055-2067.	2.6	16
71	Optical, electrical and structural properties of SiO : H films prepared from He dilution to the SiH <sub>4</sub> plasma. Journal Physics D: Applied Physics, 2009, 42, 215404.	1.3	15
72	Low temperature synthesis of spherical nano-diamond. Journal of Experimental Nanoscience, 2014, 9, 818-824.	1.3	15

#	Article	IF	CITATIONS
73	Spectroscopic and microscopic studies of self-assembled nc-Si/a-SiC thin films grown by low pressure high density spontaneous plasma processing. Physical Chemistry Chemical Physics, 2014, 16, 25421-25431.	1.3	15
74	Effect of oxygen on the optical, electrical and structural properties of mixed-phase boron doped nanocrystalline silicon oxide thin films. Applied Surface Science, 2017, 423, 1161-1168.	3.1	15
75	Rigid amorphous silicon network from hydrogenated and fluorinated precursors in ECR-CVD. Solar Energy Materials and Solar Cells, 2004, 81, 155-168.	3.0	14
76	Effect of RF power on the formation and size evolution of nC-Si quantum dots in an amorphous SiOx matrix. Journal of Materials Chemistry, 2011, 21, 7452.	6.7	14
77	Low temperature plasma processing of nc-Si/a-SiN <sub>x</sub> :H QD thin films with high carrier mobility and preferred (220) crystal orientation: a promising material for third generation solar cells. RSC Advances, 2014, 4, 36929-36939.	1.7	14
78	Preferential ã€^220〉 crystalline growth in nanocrystalline silicon films from 27.12 MHz SiH <sub>4</sub> plasma for applications in solar cells. RSC Advances, 2015, 5, 54011-54018.	1.7	14
79	Controlling the opto-electronic properties of nc-SiOx:H films by promotion of ã€^220〉 orientation in the growth of ultra-nanocrystallites at the grain boundary. Applied Surface Science, 2018, 428, 757-766.	3.1	14
80	Narrow band gap high conducting nc-Si1-xGex:H absorber layers for tandem structure nc-Si solar cells. Journal of Alloys and Compounds, 2019, 806, 1529-1535.	2.8	14
81	Electrically active boron doping in the core of Si nanocrystals by planar inductively coupled plasma CVD. Journal of Applied Physics, 2019, 126, 155305.	1.1	14
82	Advanced nanocrystallinity with widened optical gap realized via microstructural control in P-doped silicon oxide thin films used as window layer in nc-Si solar cells. Materials Chemistry and Physics, 2020, 243, 122628.	2.0	14
83	Self-assembled nc-Si-QD/a-SiC thin films from planar ICP-CVD plasma without H <sub>2</sub> -dilution: a combination of wide optical gap, high conductivity and preferred ã€~220〉 crystallographic orientation, uniquely appropriate for nc-Si solar cells. RSC Advances, 2016, 6, 3860-3869.	1.7	13
84	The growth of ZnO:Ga:Cu as new TCO film of advanced electrical, optical and structural quality. Physica E: Low-Dimensional Systems and Nanostructures, 2017, 91, 1-7.	1.3	13
85	Improvement in the optoelectronic properties of a-SiO:H films. Journal of Materials Science, 1999, 34, 1051-1054.	1.7	12
86	Effect of substrate bias on the promotion of nanocrystalline silicon growth from He-diluted SiH <sub>4</sub> plasma at low temperature. Journal of Materials Research, 2012, 27, 1303-1313.	1.2	12
87	Spectroscopic studies on nanocrystalline silicon thin films prepared from H2-diluted SiH4-plasma in inductively coupled low pressure RF PECVD. Physica E: Low-Dimensional Systems and Nanostructures, 2014, 61, 95-100.	1.3	12
88	Superior optical response of size-controlled silicon nano-crystals in a-Si:H/nc-Si:H superlattice films for multi-junction solar cells. RSC Advances, 2015, 5, 61118-61126.	1.7	12
89	Development of optimum p-nc-Si window layers for nc-Si solar cells. Physical Chemistry Chemical Physics, 2017, 19, 21357-21363.	1.3	12
90	Characterization of a-SiGe: H films prepared by rf glow discharge. Journal of Non-Crystalline Solids, 1991, 128, 172-182.	1.5	11

#	Article	IF	CITATIONS
91	Wide Band Gap Si:H at Low H-Content Prepared by Interrupted Grown and H-Plasma Treatment. Japanese Journal of Applied Physics, 1994, 33, L571-L574.	0.8	11
92	Structural investigation of nC-Si/SiOx:H thin films from He diluted (SiH4+CO2) plasma at low temperature. Applied Surface Science, 2012, 259, 477-485.	3.1	11
93	Enhanced multiferroic, magnetodielectric and electrical properties of Sm doped Lanthanum ferrite nanoparticles. Journal of Materials Science: Materials in Electronics, 2019, 30, 10694-10710.	1.1	11
94	Nanocrystallization in Si:H and quantum size effect on optical gap. Bulletin of Materials Science, 1997, 20, 9-22.	0.8	10
95	Better control over the onset of microcrystallinity in fast-growing silicon network. Journal of Materials Research, 2004, 19, 2597-2603.	1.2	10
96	Rapid synthesis of nc-Si/a-SiN <sub>x</sub> :H QD thin films by plasma processing for their cost effective applications in photonic and photovoltaic devices. RSC Advances, 2015, 5, 63572-63579.	1.7	10
97	Structural studies of n-type nc-Si–QD thin films for nc-Si solar cells. Journal of Physics and Chemistry of Solids, 2017, 111, 115-122.	1.9	10
98	Optimization in the nanostructural evolution of hydrogenated silicon germanium thin film in RF-PECVD. Physica E: Low-Dimensional Systems and Nanostructures, 2019, 111, 20-28.	1.3	10
99	Reverse Meyer-Neldel rule prevailing in the hole transport of B-doped nc-SiOx:H thin films sustaining degeneracy and performing as suitable window of nc-Si solar cells. Physica E: Low-Dimensional Systems and Nanostructures, 2021, 128, 114615.	1.3	10
100	Complex Dielectric Characteristics, ac-Conductivity, and Impedance Spectroscopy of B-Doped nc-SiO <i><sub>X</sub></i> :H Thin Films. ACS Applied Electronic Materials, 2021, 3, 1634-1647.	2.0	10
101	Evolution of microcrystalline growth pattern by ultraviolet spectroscopic ellipsometry on Si:H films prepared by Hot-Wire CVD. Solid State Communications, 2003, 128, 397-402.	0.9	9
102	Micro-photoluminescence and micro-Raman studies near the amorphous-to-microcrystalline transition in Si:H. Solid State Communications, 2003, 127, 453-456.	0.9	9
103	Development of highly conducting p-type μc-Si:H films from minor diborane doping in highly hydrogenated SiH4 plasma. Materials Letters, 2004, 58, 980-985.	1.3	9
104	Nanocrystalline silicon prepared at high growth rate using helium dilution. Bulletin of Materials Science, 2008, 31, 467-471.	0.8	9
105	Self-assembled ultra-nanocrystalline silicon films with preferred ã€^2 2 0〉 crystallographic orientation for solar cell applications. Applied Surface Science, 2015, 330, 134-141.	3.1	9
106	Opto-electronic properties of P-doped nc-Si–QD/a-SiC:H thin films as foundation layer for all-Si solar cells in superstrate configuration. Journal of Applied Physics, 2016, 120, 025102.	1.1	9
107	Highly Conducting Undoped µc-SiO:H Films Prepared by RF Glow Discharge. Japanese Journal of Applied Physics, 1999, 38, L697-L699.	0.8	8
108	Changes in Optical and Electrical Phenomena Correlated to Structural Configuration in Nanocrystalline Silicon Network. Journal of the Electrochemical Society, 2011, 158, H1138.	1.3	8

DEBAJYOTI DAS

#	Article	IF	CITATIONS
109	Self-assembled nc-Si/a-SiNx: H quantum dots thin films: An alternative solid-state light emitting material. Journal of Luminescence, 2015, 158, 11-18.	1.5	8
110	Phosphorus-doped nanocrystalline silicon-oxycarbide thin films. Journal of Alloys and Compounds, 2021, 876, 160094.	2.8	8
111	Device quality a-SiGe:H films for multijunction solar cells. Journal of Non-Crystalline Solids, 1989, 114, 552-554.	1.5	7
112	Synthesis of single-walled, bamboo-shaped and Y-junction carbon nanotubes using microwave plasma CVD on low-temperature and chemically processed catalysts. Journal of Physics and Chemistry of Solids, 2021, 152, 109971.	1.9	7
113	Influence of manganese on multiferroic and electrical properties of lanthanum ferrite nanoparticles. Materials Research Express, 2019, 6, 085032.	0.8	6
114	Nanocrystalline Diamond. , 2019, , 123-181.		6
115	Prominent c-axis oriented Si-doped ZnO thin film prepared at low substrate temperature in RF magnetron sputtering and its UV sensing in p-Si/n-SZO heterojunction structures. Journal of Physics and Chemistry of Solids, 2021, 151, 109907.	1.9	6
116	Optoelectronic and structural properties of Ge-rich narrow band gap nc-SixGe1-x absorber layer for tandem structure nc-Si solar cells. Journal of Physics and Chemistry of Solids, 2021, 154, 110055.	1.9	6
117	Evolution of nc-Si Network and the Control of Its Growth by He/H <sub>2</sub> Plasma Assistance in SiH <sub>4</sub> at PECVD. Journal of Nanoscience and Nanotechnology, 2009, 9, 5614-5621.	0.9	5
118	Low temperature growth of carbon nanotubes with aligned multiwalls by microwave plasma-CVD. AIP Conference Proceedings, 2017, , .	0.3	5
119	Growth of Nanostructured Diamond Films on Glass Substrates by Low-Temperature Microwave Plasma-Enhanced Chemical Vapor Deposition for Applications in Nanotribology. ACS Applied Nano Materials, 2022, 5, 3558-3571.	2.4	5
120	P-doped μc-Si:H films at a very low thickness and high deposition rate: Suitable for application in solar cells. Journal of Materials Research, 2003, 18, 2371-2378.	1.2	4
121	Fabrication of double barrier structures in single layer c-Si–QDs/a-SiOx films for realization of energy selective contacts for hot carrier solar cells. Journal of Applied Physics, 2017, 121, 044305.	1.1	4
122	Metastable titanium dioxide B-phase nanowire prepared by hydrothermal method. AIP Conference Proceedings, 2017, , .	0.3	4
123	Silicon nanostructure arrays prepared by single step metal assisted chemical etching from single crystal wafer. AIP Conference Proceedings, 2018, , .	0.3	4
124	Nano-diamond and Diamond-like Carbon Thin Films for Anti-Reflecting Coating Application on Silicon Solar Cells. Materials Today: Proceedings, 2018, 5, 23316-23320.	0.9	4
125	Effect of HF wet-etching and H2-plasma polishing on the low-temperature growth of carbon nanotubes on stainless-steel substrates. Journal of Physics and Chemistry of Solids, 2022, 160, 110307.	1.9	4
126	Fabrication of highly transparent diamond-like carbon anti-reflecting coating for Si solar cell application. , 2014, , .		3

8

#	Article	IF	CITATIONS
127	Investigation of the vertical electrical transport in a-Si:H/nc-Si:H superlattice thin films. Physical Chemistry Chemical Physics, 2015, 17, 17063-17068.	1.3	3
128	Growth of highly aligned vertical Si-Nanorods and random Si-Nanowires by ICP-Plasma chemical etching of c-Si wafers. AIP Conference Proceedings, 2017, , .	0.3	3
129	Highly conducting p-type nanocrystalline silicon thin films preparation without additional hydrogen dilution. AIP Conference Proceedings, 2018, , .	0.3	3
130	Growth of Multiwall Carbon Nanotubes at 300°C Using CO2 as a Weak Oxidant to (CH4+H2) Microwave Plasma. Materials Today: Proceedings, 2019, 18, 1411-1415.	0.9	3
131	Optimization of Nano-structured Tin Doped Indium Oxide Films Grown at Substrate Temperature close to the Melting Point of Tin. Materials Today: Proceedings, 2019, 18, 1304-1309.	0.9	3
132	Single-step fabrication of single-junction c-Si nano-structured solar cells by optimization of plasma etching parameters. Journal of Alloys and Compounds, 2020, 847, 155352.	2.8	3
133	Optimal H2-dilution playing key role in accomplishing significant nanocrystallinity with both Si and Ge moieties in SiGe nanocomposite thin film network. Applied Surface Science, 2022, 597, 153657.	3.1	3
134	Black silicon prepared by H2 plasma etching of single crystal wafers in PECVD. AIP Conference Proceedings, 2017, , .	0.3	2
135	Significant band gap narrowing of reduced monoclinic TiO2-B porous nanowire decorated by ternary hybrid of Cu/Cu2O-nanoparticle for efficient visible light absorption. Materials Today: Proceedings, 2019, 18, 1430-1434.	0.9	2
136	Low-temperature synthesis of conducting boron-doped nanocrystalline silicon oxide thin films as the window layer of solar cells. Current Applied Physics, 2021, 23, 42-51.	1.1	2
137	Frequency and temperature dependent electrical characteristics of P-doped nc-SiOX:H thin films. Materials Science and Engineering B: Solid-State Materials for Advanced Technology, 2021, 272, 115361.	1.7	2
138	Growth of diamond-like carbon films with significant nanocrystalline phases in a low-pressure high-density CH4 plasma in ICP-CVD: Effect of negative dc substrate bias. Applied Surface Science, 2022, 596, 153638.	3.1	2
139	Preferred C-axis oriented photoluminescent ZnO thin films prepared by RF magnetron sputtering. , 2013, , .		1
140	Structural characterization of silicon thin film superlattice grown at low temperature. Superlattices and Microstructures, 2017, 111, 385-395.	1.4	1
141	Maintaining significant ultra-nanocrystallinity in electrically conducting boron doped silicon thin layers for solar cells. AIP Conference Proceedings, 2018, , .	0.3	1
142	Vertically aligned silicon nanowire arrays prepared by silver assisted single step chemical etching. AIP Conference Proceedings, 2020, , .	0.3	1
143	Low temperature growth of a-Si/nc-Si superlattice thin films demonstrating enhanced optical absorption. AIP Conference Proceedings, 2020, , .	0.3	1
144	Synthesis of cost-effective g-C3N4/ZnO heterostructure photocatalyst for methyl orange (MO) dye degradation. AIP Conference Proceedings, 2020, , .	0.3	1

#	Article	IF	CITATIONS
145	Maintaining superior crystallinity and conductivity in boron-doped nc-Si ultra-thin films by hydrogen plasma treatment. Journal of Physics and Chemistry of Solids, 2021, 157, 110199.	1.9	1
146	Structural, Magnetic and Optical Properties of Lanthanum Ferrite Nanoparticles with Application Perspective. Advanced Science Letters, 2018, 24, 913-917.	0.2	1
147	Evolution of nanocrystalline diamond thin films by high-density low-pressure CH4 plasma in planar inductively coupled plasma CVD. AIP Conference Proceedings, 2020, , .	0.3	1
148	Synthesis and characterization of silica encapsulated magnetite nanoparticles. AIP Conference Proceedings, 2020, , .	0.3	1
149	Room temperature synthesized highly conducting B-doped nanocrystalline silicon thin films on flexible polymer substrates by ICP-CVD. Applied Surface Science, 2022, 583, 152499.	3.1	1
150	The effect of CO2 addition to the (C2H2Â+ÂH2) gas system on the low-temperature growth of diamond-like carbon (DLC) with prominent nano-diamond phase. Materials Today: Proceedings, 2022, 62, 5057-5060.	0.9	1
151	Preparation of boron doped diamond-like carbon films in a low-pressure high-density plasma in RF ICP-CVD. Materials Today: Proceedings, 2022, 62, 5105-5109.	0.9	1
152	Synthesis and characterization of organic ligand capped luminescent silicon nanoparticles. Materials Today: Proceedings, 2022, , .	0.9	1
153	Structural characteristics, impedance spectroscopy, ac-conductivity and dielectric loss studies on RF-magnetron sputtered F doped ZnO (FZO) thin films. Ceramics International, 2022, 48, 31370-31380.	2.3	1
154	Low temperature plasma synthesis of photoluminescent nanocrystalline silicon-nitride. , 2012, , .		0
155	Wide band gap nanocrystalline silicon carbide thin films prepared by ICP-CVD. , 2013, , .		0
156	Conducting intrinsic nanocrystalline silicon films with high growth rate prepared at 27.12 MHz frequency. , 2014, , .		0
157	One-step synthesis of silicon nanocrystals in aâ^'SiOx matrix at low-temperature by RF magnetron sputtering. , 2014, , .		Ο
158	Highly conducting and wide band gap phosphorous doped nc-Si–QD/a-SiC films as n-type window layers for solar cells. AIP Conference Proceedings, 2016, , .	0.3	0
159	Optimization of growth of nanocrystalline silicon germanium thin films synthesized by RF-PECVD. AIP Conference Proceedings, 2018, , .	0.3	0
160	Minimization of Reflection-Loss from Etched Nano-structures of Silicon Crystal Wafers. Materials Today: Proceedings, 2019, 18, 1324-1328.	0.9	0
161	Controlling superior crystallinity and conductivity in ultra-thin doped nc-Si layers via H2-plasma treatment for applications in nc-Si/c-Si heterojunction solar cells. AIP Conference Proceedings, 2020, ,	0.3	ο
162	Low temperature growth of highly conducting boron doped nc-Si thin films on flexible substrates. AIP Conference Proceedings, 2020, , .	0.3	0

#	Article	IF	CITATIONS
163	Biocompatible implant mimicking cartilage: A new horizon for reconstructive facial field. Artificial Organs, 2020, 44, E494-E508.	1.0	0
164	Effect of Si incorporation to produce Ge-rich nc-SixGe1-x absorber layer for nc-Si solar cells. AIP Conference Proceedings, 2020, , .	0.3	0
165	Spectroscopic studies of low-temperature synthesized nanocrystalline silicon oxy-carbide thin films. Materials Today: Proceedings, 2022, , .	0.9	0
166	Ag <sub>2</sub> O Decorated ZnO Nanorods Demonstrating Two-Step Visible-Light Photocatalytic Dye-Degradation Phenomena. IOP Conference Series: Materials Science and Engineering, 2022, 1221, 012047.	0.3	0
167	Correlation of microstructure factor with the electronic properties of nanocrystalline silicon–germanium thin films. Materials Today: Proceedings, 2022, , .	0.9	Ο
168	Intrinsic, P-doped and B-doped nanocrystalline silicon thin films grown at room temperature on flexible substrates for photovoltaic applications. Materials Today: Proceedings, 2022, , .	0.9	0
169	Diamond-Like Carbon Thin Films from Low-Pressure and High-Density CH <sub>4</sub> Plasma. IOP Conference Series: Materials Science and Engineering, 2022, 1221, 012037.	0.3	0